Influence of surface interactions on folding and forced unbinding of semiflexible chains

V. Barsegov[1] and D. Thirumalai[1,2*]

[1] *Biophysics Program, Institute for Physical Science and Technology*

[2] *Department of Chemistry and Biochemistry,*

University of Maryland, College Park, MD 20742

(Dated: May 23, 2017)

We investigate the folding and forced-unbinding transitions of adsorbed semiflexible polymer chains using theory and simulations. These processes describe, at an elementary level, a number of biologically relevant phenomena that include adhesive interactions between proteins and tethering of receptors to cell walls. The binding interface is modeled as a solid surface and the worm-like chain (WLC) is used for the semiflexible chain (SC). Using Langevin simulations, in the overdamped limit, we examine the ordering kinetics of racquet-like and toroidal structures in the presence of attractive interaction between the surface and the polymer chain. For a range of interactions, temperature, and the persistence length l_p we obtained the monomer density distribution $n(x)$ (x is the perpendicular distance of a tagged chain end from the surface) for all the relevant morphologies. There is a single peak in $n(x)$ inside the range of attractive forces b for chains in the extended conformations while in racquet and toroidal structures there is an additional peak at $x \approx b$. The simulated results for $n(x)$ are in good agreement with theory. The formation of toroids on the surface appears to be a first order transition as evidenced by the bimodal distribution in $n(x)$. The theoretical result underestimates the simulated $n(x)$ for $x \ll b$ and follows $n(x)$ closely for $x \geq b$; the density calculated exactly agrees well with $n(x)$ in the range $x \ll b$. Chain-surface interaction is probed by subjecting the surface structures to a pulling force f. The average extension $\langle x(f) \rangle$ as a function of f exhibit sigmoidal profile with sharp all-or-none transition at the unfolding force threshold $f{=}f_c$ which increases for more structured states. Simulated $\langle x(f) \rangle$ compare well with the theoretical predictions. The critical force f_c is a function of

l_s/l_c for a fixed temperature, where l_c and l_s are the length scales that express the strength of the intramolecular and SC-surface attraction, respectively. For a fixed l_s, f_c increases as l_p decreases.

I. INTRODUCTION

Interactions between biomolecules and surfaces are important in a number of biological phenomena. Binding and unbinding of proteins from macromolecular complexes are involved in the regulation of biological functions [1, 2, 3]. Adsorption of fibrinogen influences the adhesion of leukocytes, microphages or platelets. In addition, interaction between proteins, DNA and RNA are mediated by biological membranes [4, 5, 6]. In the crowded cellular conditions, protein-protein and DNA-protein interactions take place in confined geometries in which surface interactions are vital. For instance, interaction between P-selectin receptors and their specific ligands is mediated by a flat and shallow binding interface [7, 8]. Besides these situations, which are obviously relevant in biology, there are a number of situations in polymer science where interactions with surfaces are important [9, 10, 11, 12]. These include nanolubrication that involve interaction between surfaces that are mediated by polymers. Design of nanoscale materials and biologically inspired self-assembling systems also requires an understanding of how heteropolymers and biomolecules interact with surfaces. Recent advances in atomic force microscopy [7, 13, 14] has allowed a direct probe of the energetics of interaction between adsorbed proteins with other biomolecules [1, 15, 16, 17, 18, 19]. The potential applications of polymer-surface models to a number of problems has prompted us to develop a theoretical approach which can be used in conjunction with AFM experiments to decipher biomolecule-surface interactions.

There have been numerous studies of adsorption of flexible polymers adsorbed on solid surfaces which find applications in many aspects of colloidal and interface science [10, 11, 12, 20]. However, many biomolecules, including DNA, RNA, and proteins, are better described using worm-like chain (WLC) models [1, 21, 22]. Thus, it is important to provide a theoretical description of the interactions between semiflexible chains [22, 23, 24] and interfaces. The purpose

*Corresponding author phone: 301-405-4803; fax: 301-314-9404; thirum@glue.umd.edu

of this paper is to address the following specific questions: (i) It is known that DNA, a semiflexible polymer, undergoes a coil-globule transition in the presence of osmolytes or multivalent cations [23, 25]. Simulations of semiflexible chains in poor solvents [20, 26] have been used to understand the kinetics and pathways of transitions from extended conformations to collapsed toroidal structures. The coil-globule transition in stiff chains in the bulk occurs through a series of metastable racquet structures [20, 26]. How does the interaction with the surface alter the morphology and kinetics of such transitions? This question is relevant even for DNA collapse in cells where the DNA compaction takes place in the presence of interactions with their large biomolecules in restricted spaces; (ii) AFM experiments are likely to provide the most direct data for the strength of interaction between semiflexible biomolecules. In these experiments one of the molecules of interest is anchored onto the surface while force is applied to the end of the other. The unbinding force can be calculated from the force-extension profiles. These experiments raise the question, namely, what are the adhesive forces between semiflexible polymer and a surface? We address these questions using theory [12, 27, 28] and simulations for a WLC model interacting with a solid surface.

In the absence of the surface the morphologies of semiflexible chain (SC) is determined by thermal fluctuations and an interplay of the chain persistence length l_p and intramolecular condensation length $l_c{=}\sqrt{l_p k_B T/u_m}$ where T is the temperature and u_m is the effective intramolecular attractive energy per unit length [20]. In the presence of a surface another length scale $l_s{=}\sqrt{l_p k_B T/u_{ads}}$, where u_{ads} is the attractive SC-surface interaction energy per unit length, plays an essential role in the determination of the structures. The interplay of l_p, l_c, and l_s will determine the morphology of the surface-induced structures. It also follows that the response to applied force measured in terms of force-extension profiles will depend on l_p, l_c, and l_s. In this paper we explore a range of values of $k_B T$ and l_s to predict the force-extension curves for semiflexible chains in poor solvent.

II. THEORY

Consider a semiflexible chain interacting with a flat surface with the SC-surface potential being U_{ads}. Force $\mathbf{f}{=}f{\cdot}\mathbf{n}_x$ is applied to one end of the chain (Fig. 1). Equilibrium chain configuration is described using the conditional probability $G(\mathbf{x}_N, \mathbf{x}_1; \mathbf{f})$ of finding the tagged N^{th}

monomer at $\mathbf{x}_N$ given that the monomer $\mathbf{x}_1$ is anchored at the surface, where $\mathbf{x}$=$(\mathbf{r},\mathbf{n})$ includes position vector $\mathbf{r}$=(x,y,z) and orientation vector $\mathbf{n}$, respectively. Due to axial symmetry, the free end orientation is specified by the angle θ between its tangent vector and the x-axis and distance from the surface x (Fig. 1), and the conditional probability $G(x_N,\theta_N;x_1,\theta_1;f)$ can be used instead of $G(\mathbf{x}_N,\mathbf{x}_1;\mathbf{f})$. In the limit $L\to\infty$, $G(x_N,\theta_N;x_1,\theta_1;f)$ is dominated by the ground state ψ_0, so that

$$G(x_N,\theta_N;x_1,\theta_1;f)\approx\psi_0(x_1,\theta_1;f)\psi_0^{\dagger}(x_N,\theta_N;f)\exp\left[-\beta N\epsilon_0\right] \tag{1}$$

ϵ_0=E_0/N is the equilibrium free energy per monomer and β=$1/\ k_BT$. If the SC is modeled as a worm-like chain (WLC), then ψ_0 satisfies [22, 27, 28],

$$-2l_p\gamma\frac{\partial\psi_0}{\partial x}+(1-\gamma^2)\frac{\partial^2\psi_0}{\partial\gamma^2}-2\gamma\frac{\partial\psi_0}{\partial\gamma}+\beta l_p\gamma f\psi_0=\beta(u_{ads}(x)-\epsilon_0)\psi_0 \tag{2}$$

where $u_{ads}=U_{ads}/N$ is the adsorption potential per monomer and $\gamma=\cos\left[\theta\right]$ (see Fig. 1). To mimic the Lennard-Jones chain-surface attractive interaction used in the Langevin simulations (see Section III), we employ a piece-wise continuous potential, i.e. u_{ads}=∞ for x<0, u_{ads}=$-\Delta$ for $0\leq x\leq b$ and u_{ads}=0 for x>b. The monomer density of the adsorbed structures in the absence of force,

$$n(x)=\int d\theta\psi_0^2(x,\theta) \tag{3}$$

normalized as $\int dxn(x)$=N, is calculated by solving Eq. (2) without the last term $\beta l_p\gamma f\psi_0$.

The perturbative solution of Eq. (2) in the absence of the $\beta l_p\gamma f$ term, due to Kuznetsov and Sung [27], to the first order in correlation length parameter η=$(4l_p^2/\psi_0)|d^2\psi_0/dx^2|$ is outlined in Appendix A. The solution is

$$\begin{aligned}\psi_0(x) &= h(b-x)(C_1\sin\left(\frac{x\sqrt{m_1}}{2l_p}\right)+C_2\sin\left(\frac{x\sqrt{m_2}}{2l_p}\right)\\ &+ C_3\cos\left(\frac{x\sqrt{m_1}}{2l_p}\right)-C_3\cos\left(\frac{x\sqrt{m_2}}{2l_p}\right)),\\ \psi_0(x) &= C_0h(x-b)\exp\left(-\frac{x\sqrt{k}}{2l_p}\right)\end{aligned} \tag{4}$$

where $h(x)$ is the Heaviside function, and C_0, C_1, C_2 and C_3 are constant coefficients; m_1, m_2 and k are given by

$$m_{1,2}=\frac{15}{8}(2+\phi_{in})(6+\phi_{in})\left(1\mp\sqrt{1+\frac{16}{5}\frac{\phi_{in}}{6+\phi_{in}}}\right) \tag{5}$$

$$k \;=\; \frac{15}{8}(2+\phi_{out})(6+\phi_{out})\left(-1+\sqrt{1+\frac{16}{5}\frac{\phi_{out}}{6+\phi_{out}}}\right)$$

and $\phi_{in}=\beta(u_{ads}(x)-\epsilon_0)<0$, $\phi_{out}=-\epsilon_0>0$. By using two continuity requirements (A9) and the normalization, we can obtain, respectively, ϵ_0 and C_0 and one of C_1, C_2 or C_3. However, the two free constants are to be chosen such that a minimum of ϵ_0 is obtained. The minimal free energy corresponding to the ground state for $x \leq b$ is attained for (i) $C_1\neq 0$, $C_2=C_3=0$ (i.e. the state with $m=m_1$) and (ii) $C_2\neq 0$, $C_1=C_3=0$ ($m=m_2$).

Perturbative solution of Eq. (2) ignores variation of ψ_0 on θ. Indeed, when $x\gg l_p$, ψ becomes nearly isotropic, $\psi(x,\theta)=\psi(x)$. However, when $x\sim b\ll l_p$, ψ_0 should strongly depend on the angle $\Theta = \pi/2+\theta$ between free end of the chain and the surface (Fig. 1). In this range $-\gamma\partial/\partial x\to\Theta\partial/\partial x$, $(1-\gamma^2)\,\partial^2/\partial\gamma^2\to\partial^2/\partial\Theta^2$, $\gamma\partial\,/\partial\gamma\to 0$, $\gamma f\to-\Theta f$ and Eq. (2) simplifies, i.e.

$$\Theta\frac{\partial\psi_0}{\partial x}+\frac{1}{2l_p}\frac{\partial^2\psi_0}{\partial\Theta^2}-\frac{1}{2}\Theta f\psi_0=\frac{\beta}{2l_p}(u_{ads}(x)-\epsilon_0)\psi_0. \tag{6}$$

The methodology for solving Eq. (6) has been presented by Semenov in Ref. [28] and is outlined in Appendix B. The general solution for $x>b$ ($u_{ads}=0$) is

$$\psi_0(x,\Theta)=\sum_{n=0,1}C_n x^{1/6-n}\Psi\left(n-\frac{1}{6},\frac{2}{3},\frac{2l_p\Theta^3}{9x}\right) \tag{7}$$

where C_0, C_1 are constants and the confluent hypergeometric function $\Psi(\chi,\omega,z)$ is $\Psi(\chi,\omega,z)\equiv\frac{1}{\Gamma(\chi)}\int_0^\infty d\tau\;\tau^{\chi-1}(1+\tau)^{\omega-\chi-1}e^{-\tau z}$ where $\Gamma(\chi)\equiv\int_0^\infty d\tau\tau^{\chi-1}\exp[-\tau]$ is Gamma function [29]. To describe the chain in the range $x\leq b$, we assume that ψ_0 is of the form (7) and C_0 and C_1 depend on x. Substituting Eq. (7) into Eq. (6), we obtain:

$$\begin{aligned}\frac{dC_0}{dx} &= \phi(x)\left(\frac{2l_p}{x}\right)^{1/3}\left(F_{00}C_0+F_{01}x^{-1}C_1\right)\\ \frac{dC_1}{dx} &= \phi(x)\left(\frac{2l_p}{x}\right)^{1/3}\left(F_{10}xC_0+F_{11}C_1\right)\end{aligned} \tag{8}$$

where $F_{nm}\equiv(g_m/\kappa,f_n)/(f_n,f_n)$, $n,m=0,1$, and $(g_n,g_m)\equiv\int_{-\infty}^{\infty}d\kappa\kappa e^{-\kappa^3/9}g_n(\kappa)\;g_m(\kappa)$ (see Eq. (B2)). We solve Eqs. (8) subject to the condition $\phi(x)=\phi_{in}$ for $x\leq b$ and $\phi(x)=\phi_{out}$ for $x>b$. From the solutions of Eqs. (8) in Appendix B we obtain:

$$\begin{aligned}C_1^{in}(x) &= c_2 e^{\frac{3}{2}\sqrt{-D}x^{\frac{2}{3}}}\left(-3\sqrt{-D}x^{\frac{2}{3}}\right)^{\frac{3}{2}}\Phi\left(\rho+\frac{3}{2},\frac{5}{2},-3\sqrt{-D}x^{\frac{2}{3}}\right)h(b-x)\\ C_1^{out}(x) &= c_1 e^{-\frac{3}{2}\sqrt{-D}x^{\frac{2}{3}}}\Phi\left(\rho,-\frac{1}{2},3\sqrt{-D}x^{\frac{2}{3}}\right)h(x-b)\end{aligned} \tag{9}$$

where $\sqrt{-D} = \phi_{out}(2l_p)^{\frac{1}{3}}\sqrt{F_{01}F_{10} - F_{11}F_{00}}$ and $h(x)$ is Heaviside step function. In Eq. (9) the Kummer function $\Phi(k,l,x)$ is defined by $\Phi(k,l,x) \equiv 1 + \sum_{m=1}^{\infty} \frac{(k)_m}{(l)_m} \frac{x^m}{m!}$ with $(k)_0=1$, $(k)_1=k$ and $(k)_m=k(k+1)\ldots(k+m-1)$ [29]. We get $C_0(x)$ by substituting Eqs. (9) for C_1^{in} and C_1^{out} into the second Eq. (8) and $\psi_0(x,\Theta;f)$ can now be obtained by using Eq. (7)).

In the presence of pulling force, ψ_0 is nearly isotropic, i.e. $\psi_0(x,\theta;f) \approx \psi_0(x;f)$. This allows us to analyze force-extension profiles by employing perturbative treatment outlined above. Solution to Eq. (2) is given by

$$\psi_0(x;f) = \psi_0(x) e^{\frac{1}{2}\beta f x} \tag{10}$$

where $\psi_0(x)$ is given by Eqs. (4). The average extension as a function of applied force can be computed using

$$\langle x(f) \rangle \equiv \frac{1}{\beta} \frac{1}{Z(f)} \frac{d}{df} Z(f) \tag{11}$$

where the partition function $Z(f)$ is $Z(f) = \int d\theta_N \int d\theta_1 \int dx_N \int dx_1 G(x_N, \theta_N; x_1, \theta_1; f)$.

The perturbation theory is strictly valid only when the condensation length $l_c \gg l_p$. In practice we find that the first order perturbation theory gives results that are in very good agreement with simulations even when $l_c \sim l_p$. Kuznetsov and Sung also discovered that the perturbation theory is remarkably successful outside the regime of applicability [27].

III. LANGEVIN DYNAMICS SIMULATIONS

We model a semiflexible chain (SC) by N=100 connected beads of bond length a and the contour length L=100a. In the absence of U_{ads} and f=0, we assume that the dynamics is governed by the overdamped Langevin equation:

$$\xi \frac{d}{dt} \mathbf{x}_j = -\frac{\partial U}{\partial \mathbf{x}_j} + \mathbf{g}_j(t) \tag{12}$$

where ξ is the friction coefficient, $U = U_{chain} = U_{bond} + U_{bend} + U_{LJ}$ is chain internal energy due to bond potential U_{bond}, bend potential U_{bend} and interbead interaction potential U_{LJ} (hydrodynamic interactions are ignored). The random force $\mathbf{g}_j(t)$ obeys Gaussian statistics,

$$\langle \mathbf{g}_j(t) \rangle = 0, \quad \langle \mathbf{g}_i(t) \mathbf{g}_j(t') \rangle = 6 k_B T \xi \delta_{ij} \delta(t - t') \tag{13}$$

We solve Eq. (12) for each $\mathbf{x}_j$ with unit tangent vector $\mathbf{u}_j$=$(\mathbf{x}_{j+1}-\mathbf{x}_j)/a$, where j=$1, 2, \ldots, N$. The stretching potential U_{bond} is

$$U_{bond} = \frac{A}{2\sigma^2}\sum_{j=1}^{N-1}(|\mathbf{x}_j - \mathbf{x}_{j+1}|^2 - \sigma)^2, \tag{14}$$

where A and σ are constants, and

$$U_{bend} = \frac{S}{2}\sum_{j=1}^{N-1}(1+\cos[\varphi_{j,j+1}])^2 \tag{15}$$

where the constant S is a measure of chain stiffnes, and $\cos[\varphi_{j,j+1}]$= $(\mathbf{x}_{j+1}-\mathbf{x}_j)(\mathbf{x}_{j-1}-\mathbf{x}_j)/\sigma^2$ is the bend angle. The interaction between beads is given by the 12-6 Lennard-Jones potential,

$$U_{LJ} = B\sum_{i<j}\left[\left(\frac{\sigma}{\Delta\mathbf{x}_{ij}}\right)^{12} - 2\left(\frac{\sigma}{\Delta\mathbf{x}_{ij}}\right)^{6}\right] \tag{16}$$

where $\Delta\mathbf{x}_{ij}$ is the distance between beads i and j, and B is the magnitude of interaction. U_{LJ} is an effective interaction that accounts for excluded volume interactions and counterion induced attraction which in DNA is due to screening of the charges. The persistence length of the chain l_p can be roughly estimated by using l_p=$a/(1-\cos[\langle\varphi_{j,j+1}\rangle])$ where $\langle\varphi_{j,j+1}\rangle$=$(N-1)^{-1}\sum_{j=1}^{N-1}\varphi_{j,j+1}$ is the average angle between adjacent beeds.

Similar models have been used in previous studies to probe the chain collapse in poor solvents [20, 26]. In the presence of the adsorbing surface the motion of j-th bead is governed by Eq. (12) with U=U_{chain}+U_{ads}, where U_{ads} is the surface-SC potential,

$$U_{ads} = \Delta\sum_{i}\left[\left(\frac{b}{\Delta\mathbf{x}_i}\right)^{12} - 2\left(\frac{b}{\Delta\mathbf{x}_i}\right)^{6}\right]. \tag{17}$$

In Eq. (17) $\Delta\mathbf{x}_i$ is the bead-surface distance and Δ and b are, respectively, the depth and range of the attractive forces. We set $B = 1.0$, σ=a=1 and b=$3a$, and use A=$400B$, S=$30B$, $60B$, $120B$ and Δ=$1.5B$, $2.0B$, $2.5B$. This makes U_{LJ}, U_{bond}, U_{bend} and U_{ads} to scale in units of ϵ_h=k_BT and ϵ_l=σ is the unit length. The choice A=$400B$ allows for 5 percent of thermal fluctuations in the bond distance and permits us to run simulations with longer time steps without affecting bond relaxation time. The unit of time is τ=$\xi\sigma^2/\epsilon_h$, where ξ= 44.0 is the friction coefficient of the chain in water at $T = 300K$. The system of equations (12) is integrated with a step size δt=$2\times10^{-2}\tau$ and the total time is t=$N_{tot}\delta t$ where N_{tot} is the number of integration steps. We express time either in units of τ or in terms of N_{tot}.

IV. RESULTS

A. Surface-induced structural transitions:

It is known that in the absence of the surface SC undergoes a collapse transition when the solvent is poor i.e., when the attractive monomer-monomer interactions dominate (Eq. (16)) so that $l_c > l_p$. The collapse is a result of a competition between intramolecular attraction and bending energy due to chain stiffness. Unlike in flexible polymers, the low energy collapsed conformation is a torus which maximizes intramolecular contacts and minimizes the bending penalty. Before simulating the force-extension curves of adsorbed SC it is necessary to characterize the structures that are obtained when interacting with the surface.

To simulate the low free energy structures that result in the presence of the surface, we first thermalized an extended chain at high temperature k_BT=3.0 for N_{tot}=1×10^6 steps. By gradually decreasing the temperature bulk structures were thermalized for $(1-10)\times10^7$ steps and used in adsorption experiments. Interactions with the attractive surface was switched on at distance $\Delta x = 2b$ away from the bead with shortest x and the SC was adsorbed onto the surface one bead at a time. The structures were allowed to relax for $\sim 1-20\times10^6$ steps depending on k_BT, S and Δ. Progress of adsorption was monitored by analyzing time traces of U_{LJ}, U_{ads}, U, and the radius of gyration R_g of the SC. We generated 500 adsorbed structures at k_BT=1.0, 1.25 and 1.5 for $S = 30B$, $60B$, $120B$ and $\Delta = 1.5B$, $2.0B$ and $2.5B$.

Typical structures are presented in Fig. 2. Geometry of the SC adsorbed onto the surface ranges from partially or fully extended configuration with $l_p/a \approx 18$ to partially structured one-, two- and three-racquet states with $l_p/a \approx 16.0$, 15.5 and 15.0, respectively, to fully ordered toroidal states with $l_p/a \approx 13.5$. Similar structures have been observed in recent studies of collapse of semiflexible chains in the bulk [20, 26]. For the interaction parameters used in our simulations $l_s/l_c \sim o(1)$. Thus, the attractive SC-surface interaction facilitates adsorption of the SC without significantly altering its morphology compared to the bulk case. For $l_s \gg l_c$ the lowest free energy structures are extended.

To compare the kinetics of structure formation on the surface and in the bulk we also simulated collapsed structures in the absence of the adsorbing surface. By analyzing the temporal profiles of R_g, U_{LJ} and l_p, we found that on average, chains attain structured configurations on a faster timescale when adsorbed on the surface. The search for the ground (toroidal) state is

more efficient when the chain is constrained to evolve on the two-dimensional surface where the SC quickly minimizes its free energy in reduced d=2-space by sliding surface motion (lateral diffusion).

B. Kinetics of surface-induced ordering:

Typically, surface-induced ordered structures form by a two step process $B_0 \rightarrow S_0 \rightarrow S_t$. Starting from the bulk state B_0, extended surface transient S_0 emerges during the fast first step with the $B_0 \rightarrow S_0$ transition occuring within $N_{tot}=1-3\times10^6$. In the slower second step $S_0 \rightarrow S_t$, extended transient structures explore the free energy landscape in search of the toroidal state S_t which occurs in about $3-20\times10^6$ steps depending on S, Δ and temperature. Transition from S_0 to S_t is realized via rapid formation of either a surface loop or an intermediate toroid-like motif with larger R_g (smaller winding number) or through a sequence of longer lived racquet states $S_0 \rightarrow S_1 \rightarrow \ldots \rightarrow S_t$, where S_n, n=0,1,2,... denotes conformations with number of racquets equal to zero (extended chain) one, two, etc.

The number of "metastable" racquets depends on chain flexibility. We observed configurations with n=6 for S=30B and k_BT=1.25. Simulated profiles of R_g, U_{LJ}, U_{ads} and U indicate that evolution from extended to toroidal states follows several pathways. Four out of five simulation runs followed the scheme outlined above. Similar diverse pathways have been observed by Noguchi and Yoshikawa [20] who recorded the lifetime of intermediates species for about $N_{tot}=2.0\times10^5$. Our results indicate that attractive surface forces increase the lifetimes of metastable intermediates for stiff chains at low temperature. In few simulation runs toroidal structures were not observed during as many as 20×10^6 steps. Hence, attractive surface forces facilitate formation of toroidal state primarily when formation of toroid-like intermediate motif is involved.

The dynamics of R_g, U_{LJ}, U_{ads} and U for the structures in Fig. 2 show that increasingly more ordered states are also energetically favorable (Fig. 3). R_g, U and U_{LJ} decrease and U_{abs} increases in the sequence $S_0 \rightarrow S_1 \rightarrow S_2 \rightarrow S_3 \rightarrow S_t$. R_g fluctuates around larger values for extended states. Variations in U_{LJ}, U_{ads} and U increasing in the sequence of $S_1 \rightarrow S_2 \rightarrow S_3 \rightarrow S_t$ transitions are due to formation of SC-surface contacts. For the structures in Fig. 2, the formation of S_1 at $N_{tot} \approx 2.0\times10^6$ is mediated by a surface-loop motif followed by slow sliding motion; S_2 forms

early at $N_{tot}\approx 5.0\times10^5$ and remains unchanged (time dependence of R_g or U_{LJ}). The dynamics of U_{LJ}, U_{ads} and U show formation of S_3 via S_1 at $N_{tot}\approx 1.0\times10^5$ followed by transition $S_1\rightarrow S_3$ at $N_{tot}\approx 7.0\times10^6$. Similarly, traces of same quantities for S_t point at three step transition, $S_0\rightarrow S_1\rightarrow S_3\rightarrow S_t$ occuring respectively at $N_{tot}\approx 5.0\times10^5$, 1.5×10^6 and 4.0×10^6, followed by chain compaction due sliding motion.

In agreement with theoretical arguments [28] monomer profiles of stiff chains (S=120B, $l_p/b \gg 1$) are described by the succession of short near-surface loops of length $\ll l_p/a$ between chain-surface contact and by the combination of short and long loops of the length $\gg l_p/a$ for S=30B and $l_p/b\sim1$. Decrease in l_p/b and temperature favors the formation of chain-surface contacts by enabling more beads to be inside the range of surface forces. This results in the formation of higher ordered states S_4, S_5, S_6 and S_t. In contrast, at higher temperatures and increased Δ and S, surface structures with increased conformational free energy become unstable and unfold into extended configurations (data are not shown). We quantified the geometry of surface structures (Fig. 2) by binning bead-surface distances x_j into the density histogram $n(x)$. The monomer density profiles for Δ=1.5B and k_bT=1.0 are compared in Fig. 4 for S=70B (left) and S=50B (right panels). Transition from less structured to more structured states is accompanied by an increased ratio of the number of bead-bead to bead-surface contacts. The density distribution $n(x)$ is single-peaked at x=$b/2$ and decays to zero as $x\rightarrow b$ for extended states and increases its density at $x\approx b$ in the sequence $S_1\rightarrow S_2\rightarrow S_3\rightarrow S_t$.

C. Forced unfolding of surface adsorbed structures:

To unfold the surface-ordered structures, these structures were initially allowed to thermalize at k_BT=1.0 for N_{tot}=2×10^6. We then ancored the C-terminus of the chain at the surface and pulled its N-terminus with constant force f via the harmonic spring with the spring constant k_{sp}=$0.36pNnm^{-1}$ in the direction perpendicular to the surface. Simulation runs were terminated after evolution of chain extension $x(N_{tot})$ had reached equilibrium. $x(N_{tot})$ of the structures of Fig. 2 are presented in Fig. 5 for f=$9.75pN$, $18.3pN$, $24.4pN$ and $30.5pN$. Chain extension reaches saturation plateau in the first 8×10^7 steps as the chain restoring force approaches f. Not unexpectedly, the unfolding threshold force increases as the extent of ordering decreases in the sequence $S_0\rightarrow S_1\rightarrow S_2\rightarrow S_3\rightarrow S_t$. At f=$9.75pN$ only S_0 unfolds in 1.0×10^7 steps. When the

force is increased to f=18.3pN, S_0, S_1, S_2 and S_3 unbind from the surface in 3.5×10^7, 3.6×10^7, 4.0×10^7 and 6.0×10^7 steps, respectively. At f=24.4pN all structures reach the stretched state in 2−4×10^7 steps. From the dynamical trajectories of x obtained for Δ=1.5B and k_BT=1.0, we constructed the average extension $\langle x\rangle$ as a function of f. In Fig. 6 we compare $\langle x\rangle$ vs f traces for extended, one-racquet, three-racquet and toroidal structures of Fig. 2 (S=120B, top panel) and more flexible four-, five- and seven-racquet and toroidal conformations obtained for S=30B. Unbinding of surface-anchored structures undergo a highly cooperative all-or-none transition as the unfolding force threshold f=f_c is increased from 7.3−15.8pN (S=120B) to 15.9−17.7pN (S=30B) for more compact racquet and toroidal states.

D. Comparison between theory and simulations:

We analyzed the simulation results for the monomer density and the averaged extension as a function of the pulling force by using perturbative treatment (see Eqs. (3)-(5)) in the entire range of x<L. For the proximal limit x≪l_p<L we use the exact expressions in Eqs. (7) and (9). Density distributions and force-extension profiles for the extended conformation were approximated by chosing the ground state with m=m_1 (m_1<m_2, see Eq. (5)). The choice m=m_1 corresponds to isotropic-like unstructured surface state with no prefered orientation of the chain beads. Histograms of structured two-, three-racquet and toroidal conformations were analyzed with the choice m=m_2 corresponding to nematic-like ordered states [27]. To account for the difference between the shape of attractive potential U_{ads} used in the simulations and the theoretical calculation we used, in the actual fit, the rescaled potential depth Δ_T=$r\Delta_{sim}$ for the same range b_T=b_{sim}=1, where r=$(b\Delta_T)^{-1}\int_0^\infty dx u_{ads}(x)$ is the ratio between volume of Lennard-Jones attractive layer and $b\Delta_T$ used in theory. The density profiles $n(x)$ for known values of b, k_BT and Δ_T were fitted to the simulated monomer density histograms and force-extension profiles to obtain parameters ϵ_0 (Eq. (1)) and l_p. The theoretical results for the density $n(x)$ and the average extension $\langle x(f)\rangle$ computed from Eqs. (3) and (11), respectively, using these parameters are shown in Figs. 4 and 6.

Monomer density distributions: Although the theoretical results for $n(x)$ slightly underestimate the simulated density for structured states for b<x/a<1.5 and underestimates it for x/a>1.6, the agreement between perturbation theory and simulation data is surprisingly good

in the range of $x/a \leq b$ (Fig. 4). The agreement between theory and simulations improves for more structured racquet and toroidal conformations. In particular, the theoretical profiles capture the positions of density peaks both inside the layer at $x/a \approx 0.5$ and at the boundary $x/a \approx b$. Although there is some residual density at large x/a due to thermal fluctuations of chain ends, especially for less structured extended and racquet configurations, the ground state dominance approximation is clearly valid. The theoretically estimated conformational free energy per monomer and persistence length for structures $S_0 \to S_2 \to S_3 \to S_t$ of Fig. 4 decrease respectively as $\epsilon_0/k_BT \approx -0.21 \to -0.23 \to -0.24 \to -0.25$ and $l_p/a \approx 11.7 \to 11.2 \to 10.4 \to 10.2$ (for $k_BT=1.0$, left panels), and $\epsilon_0/k_BT \approx -0.23 \to -0.25 \to -0.26 \to -0.27$ and $l_p/a \approx 11.3 \to 11.0 \to 10.2 \to 10.1$ (for $k_BT=1.25$, right panels). Not surprisingly, both ϵ_0 and l_p decrease for the same structures as k_BT is increased because of enhanced chain flexibility. In the proximal region, the exact calculation of $n(s)$ for $0 \leq x/a \leq 0.5$ for the same structure sequence shows a better agreement with the simulated results. The fit parameters are $\epsilon_0/k_BT \approx -0.2 \to -0.24 \to -0.25 \to -0.28$ and $l_p/a \approx 12.3 \to 11.8 \to 11.0 \to 10.8$ for $k_BT=1.0$, and $\epsilon_0/k_BT \approx -0.19 \to -0.22 \to -0.24 \to -0.26$ and $l_p/a \approx 12.0 \to 11.6 \to 10.8 \to 10.6$ for $k_BT=1.25$.

Force-extension curves: Apart from small deviations around the unfolding threshold forces for all simulated surface structures, the fit of theoretical curves of the average extension vs pulling force to simulated data points shows excellent agreement between theory and simulations. The theoretical $\langle x(f) \rangle$ curves calculated using perturbation theory follow closely the simulated force-extension profiles both for $S=120B$ and $S=30B$ especially below ($x/L \leq 0.1$) and above ($x/L \geq 0.9$). The unbinding threshold forces increase as $7.5pN < 10.5pN < 12.5pN < 16.5pN$ in the sequence $S_0 \to S_1 \to S_3 \to S_t$ ($S=120B$, top panel in Fig. 6) and as $15pN < 15.5pN < 16.5pN < 17.5pN$ in the sequence $S_4 \to S_5 \to S_7 \to S_t$ ($S=30B$, bottom panel in Fig. 6). This implies that more flexible and/or more structured surface chains are harder to unfold. However, "all-or-none" type of simulated unfolding transition shows sharper growth than predicted by the theory. The theoretically estimated conformational free energy per monomer and persistence length for structures $S_0 \to S_1 \to S_3 \to S_t$ decrease respectively as $\epsilon_0/k_BT \approx -0.12 \to -0.17 \to -0.20 \to -0.22$ and $l_p/a \approx 15 \to 14.5 \to 14.25 \to 12.1$ (top panel). For the structures $S_4 \to S_5 \to S_7 \to S_t$, ϵ_0 decreases as $\epsilon_0/k_BT \approx -0.134 \to -0.136 \to -0.141 \to -0.148$ and $l_p/a \approx 8.2 \to 8.1 \to 8.0 \to 7.9$ (bottom panel). Here too, increased chain flexibility decreases l_p and lowers ϵ_0.

V. CONCLUSIONS

To provide insights into interactions between biomolecules interacting with membranes we have considered collapse and forced-unbinding of semiflexible chains (SC) in the presence of an adsorbing surface. The interaction of SC modeled using WLC, which describes well many of the physical properties of DNA [19], RNA [30], and proteins [31], with a surface into which the SC can adsorb, is studied using theory and simulations. The morphologies of the SC in the presence of an adsorbing potential is described in terms of three length scales, namely, l_p, l_s, and l_c. By restricting ourselves to $l_c \approx l_s$ we have studied the effect of interaction with the surface on coil-toroidal transition in DNA like chains. The simulations show that the rate of toroid formation is impeded compared to the bulk because interaction with the surface stabilizes many metastable racquet-like structures (Fig. 1). The simulated equilibrium density profiles show that as the range of surface-SC interaction increases and temperature decreases, which leads to a decrease in l_p/l_s, ordered structures form. The peak of $n(x)$ at $x \approx b$ (the range of interaction) grows as l_p decreases. The bimodality in the $n(x)$ distribution function suggests that the surface-induced toroid formation is a first order transition. The perturbative calculation reproduces qualitatively all the features in the simulated density profiles.

We also considered the peeling and unbinding of adsorbed structures by applying force. These results, which are of direct relevance to AFM experiments [32], show that the forced-unbinding transition is surprisingly highly cooperative. For all structures (racquet-like and toroids) unbinding occurs over a narrow force range. The magnitude of the critical force f_c for a fixed value of T and l_s increases as l_p decreases. From general considerations we expect that f_c should be described by a scaling a function $g(y)$ where $y = l_s/l_p$ for a fixed T. When $y < y_c$ (a critical value), then adsorbtion is not free energetically favored. When $y > y_c$, then f_c should increase by an increasing function of y. The increase in f_c can be achieved either by increasing l_s for a fixed l_p or by decreasing l_p for fixed l_s. Additional work is required to elucidate the nature of the scaling function $g(y)$. Quite surprisingly, we find that the force-extension profiles can be calculated by using a simple perturbation theory even though the nature of the unbinding transition is abrupt. The present work shows that global properties of force-extension characteristics of adsorbed biomolecules can be nearly quantitatively predicted using the proposed theory.

It is now well established that elastic response of DNA, in the absence of interaction with surfaces, depends sensitively on the nature and concentration of counterions [32, 33]. Our work shows that the force-extension curves in the presence of a surface to which DNA is bound depends not only on l_s but also on the morphology of the adsorbed structures. The novel prediction that forced unbinding should occur cooperatively by a first-order phase transition can be probed using single molecule experiments.

Acknowledgments

This work was supported in part by a grant from the National Science Foundation through NSF CHE05-14056. We would like to thank Changbong Hyeon for many useful discussions.

APPENDIX A: PERTURBATIVE TREATMENT OF ADSORBED CHAIN STATISTICS

We expand ψ_0 (Eq. (1)) in terms of the Legendre polynomials, i.e.

$$\psi_0(x,\theta) = \sum_{i=0}^{\infty} \psi_i(x) P_i(\cos[\theta]) \tag{A1}$$

By using the following equations,

$$\frac{d}{d\gamma}P_i(\gamma) = -i(i+1)P_i(\gamma) \quad \text{and} \quad P_1(\gamma)P_i(\gamma) = \frac{(i+1)P_{i+1}(\gamma) + iP_{i-1}(\gamma)}{2i+1} \tag{A2}$$

we transform Eq. (2) without term $\beta l_p \gamma f \psi_0$ into ($i \geq 0$)

$$\frac{i(i+1) + \beta(u_{ads} - \epsilon_0)}{2l_p}\psi_i(x) = -\frac{i}{2i-1}\frac{d\psi_{i-1}(x)}{dx} - \frac{i+1}{2i+3}\frac{d\psi_{i+1}(x)}{dx} \tag{A3}$$

To the first few orders we have:

$$\begin{aligned}
\psi_0 &= \frac{2l_p}{3\beta(u_{ads}-\epsilon_0)}\frac{d\psi_1}{dx} \qquad (i=0), \\
\psi_1 &= -\frac{2l_p}{2+\beta(u_{ads}-\epsilon_0)}\frac{d\psi_0}{dx} - \frac{4l_p}{5(2+\beta(u_{ads}-\epsilon_0))}\frac{d\psi_2}{dx} \qquad (i=1), \\
\psi_2 &= -\frac{4l_p}{3(6+\beta(u_{ads}-\epsilon_0))}\frac{d\psi_1}{dx} - \frac{6l_p}{7(6+\beta(u_{ads}-\epsilon_0))}\frac{d\psi_3}{dx} \qquad (i=2),
\end{aligned} \tag{A4}$$

ψ_1 is given by the second Eq. (A4) with the second term determined by ψ_2 which is of the order of $8l_p^3 d^3\psi_0/dx^3$. Neglecting this order for $\eta \ll 1$ we obtain:

$$\psi_1 \approx -\frac{2l_p}{2+\beta(u_{ads}-\epsilon_0)}\frac{d\psi_0}{dx} \tag{A5}$$

Including the second term in the third Eq. (A4) and using Eq. (A5) we obtain the first-order perturbation equation for ψ_1,

$$\psi_1 \approx -\frac{2l_p}{2+\phi}\frac{d\psi_0}{dx} - \frac{4l_p}{5(2+\phi)}\frac{d}{dx}\left[\frac{4l_p}{3(6+\phi)}\frac{d}{dx}\left(\frac{2l_p}{2+\phi}\frac{d\psi_0}{dx}\right)\right] \tag{A6}$$

where $\phi = \beta(u_{ads}-\epsilon_0)$. Substitute Eq. (A6) into the first Eq. (A4) we arrive at the first-order perturbative equation for ψ_0:

$$\frac{64l_p^4}{45\phi(2+\phi)^2(6+\phi)}\frac{d^4\psi_0}{dx^4} + \frac{4l_p^2}{3\phi(2+\phi)}\frac{d^2\psi_0}{dx^2} - \psi_0 = 0 \tag{A7}$$

For the class of potentials considered here, the physical solution of Eq. (A7) that satisfies the boundary conditions,

$$\psi_0(x=0)=0, \quad \psi_0(x\to\infty)\to 0, \quad \frac{d^n}{dx^n}\psi_0|_{x\to\infty}\to 0, \quad n=1,2,\ldots \tag{A8}$$

continuity requirements at $x=b$,

$$\psi_0(x\to b-0)=\psi_0(x\to b+0), \quad \frac{d}{dx}\psi_0|_{x\to b-0}=\frac{d}{dx}\psi_0|_{x\to b+0} \tag{A9}$$

and normalization condition is given by Eq. (4).

APPENDIX B: EXACT TREATMENT OF THE CHAIN DISTRIBUTION IN THE PROXIMAL RANGE

Let us first consider the non-adsorbed chain in the presence of weak potential $u_{ads}\to 0$. Assuming a self-similar distribution, $\psi_0(x,\Theta) = x^\alpha g(\kappa)$ where $\kappa = \Theta(2l_p/x)^{1/3}$, we rewrite Eq. (6) with $u_{ads}=\epsilon_0=0$ as an eigenvalue problem for $g(\kappa)$,

$$-\frac{1}{\kappa}\frac{\partial^2 g}{\partial\kappa^2} + \frac{\kappa}{3}\frac{\partial g}{\partial\kappa} = \alpha g \tag{B1}$$

Upon substitution $z=\kappa^3/9$, Eq. (B1) reduces to the following equation:

$$z\frac{d^2 g}{dz^2} + \left(\frac{2}{3}-z\right)\frac{dg}{dz} + \alpha g = 0 \tag{B2}$$

Under condition $g(z{\to}\infty){\to}0$ the only solution to Eq. (B2) is $g(z){\sim}\Psi(-\alpha, 2/3, z)$ where $\Psi(\chi,\omega,z)$ and $\Gamma(\chi)$ are defined in the main text. $\psi(x{\to}0,\Theta{<}0){\to}0$ defines the spectrum of eigenvalues $\alpha_n{=}1/6{-}n$, where $n = 0,{\pm}1,{\pm}2,\ldots$ (see Appendix B in Ref. [28]). The requirement that ψ does not have knots is satisfied for $n = 0$ ($\alpha{=}1/6$) and $n{=}1$ ($\alpha{=}{-}5/6$), and the general solution for $u_{ads}{=}0$ in the region $x{>}b$ is given by Eq. (7) of the main text.

To solve Eqs. (8) we substitute C_0 from the second equation into the first equation and multiply by $x^{2/3}$. We obtain:

$$x^{4/3}\frac{d^2C_1}{dx^2} - \frac{2}{3}x^{1/3}\frac{dC_1}{dx} + (\bar{F}_{11} + Dx^{2/3})C_1 = 0 \tag{B3}$$

where $D = \bar{F}_{00}\bar{F}_{11} - \bar{F}_{01}\bar{F}_{10}$ and $\bar{F}_{nm} = F_{nm}\phi(2l_p)^{1/3}$, $n, m = 0, 1$. Substituting $y = x^{1/3}$ into Eq. (B3) and multiplying it by y^2, we get:

$$y^2\frac{d^2C_1}{dy^2} - 2y\frac{dC_1}{dy} + y^2(9\bar{F}_{11} + 9Dy^2)C_1 = 0 \tag{B4}$$

Using $z = y^2$ allows us to rewrite Eq. (B4) as

$$\gamma_2 z\frac{d^2C_1}{dz^2} + \beta_1\frac{dC_1}{dz} + (\gamma_0 z + \beta_0)C_1 = 0 \tag{B5}$$

where $\gamma_0{=}9D$, $\beta_0{=}9\bar{F}_{11}$, $\beta_1{=}{-}4$ and $\gamma_2{=}4$. The general solution of Eq. (B5) is given by

$$C_1(x) = e^{\frac{3}{2}\sqrt{-D}x^{\frac{2}{3}}}[c_1\Phi(\rho, -\frac{1}{2}, -3\sqrt{-D}x^{\frac{2}{3}}) + c_2(-3\sqrt{-D}x^{\frac{2}{3}})^{\frac{3}{2}}\Phi(\rho + \frac{3}{2}, \frac{5}{2}, -3\sqrt{-D}x^{\frac{2}{3}})] \tag{B6}$$

where c_1, c_2 are constants and $\rho{=}(3\bar{F}_{11}{-}2\sqrt{-D})/4\sqrt{-D}$. In Eq. (B6) $\Phi(k,l,x)$ is the Kummer series defined in the text. In the range $0{\le}x{\le}b$, $\psi_1(x,\Theta{=}0)$ diverges as $x{\to}0$. To avoid this divergence we require that $C_1(x{=}0){=}0$. This is satisfied when $c_1{=}0$. To insure that $C_1(x){\to}0$ as $x{\to}\infty$ for $x{>}b$, we set $c_2{=}0$. Substituting $\phi{=}\phi_{in}$ and $\phi{=}\phi_{out}$ into solutions for $0{\le}x{\le}b$ and $x{>}b$ and using formulas $\Phi(k,l,x){=}e^x\Phi(l-k,l,x)$, $\frac{d^m}{dx^m}\Phi(k,l,x){=}\frac{(k)_m}{(l)_m}\Phi(k+m,l+m,x)$ we obtain Eqs. (9).

---

[1] Liphardt, G.; Smith, D.; Bustamante, C. Curr. Opin. Struct. Biol. 2000, 10, 279; Allemand, J.-F.; Bensimon, D.; Croquette, V. ibid 2003, 13, 266

[2] Yin, H.; Wang, M. D.; Svoboda, K.; Landick, R.; Block, S. M.; Gelles, J. Science 1995, 270, 1653; Bianco, P. R.; Brewer, L. R.; Corzett, M.; Balhorn, R.; Yeh, Y.; Kowalczykowski, S. C.; Baskin, R. J. Nature 2001, 409, 374

[3] Alberts, B. Molecular Biology of the Cell, 1st ed.; Garland Publishing: New York, 1994

[4] Labeit, S.; Kolmerer, B. Science 1995, 270, 293; Minajeva, A.; Kulke, M.; Fernandez, J. M.; Linke, W. A. Biophys. J. 2001, 80, 1442

[5] Henrickson, S. E.; Misakian, M.; Robertson B.; Kasianowicz, J. J. Phys. Rev. Lett. 2000, 85, 3057; Kasianowicz, J. J.; Brandin, E.; Branton, D.; Deamer, D. W. Proc. Natl. Acad. Sci. USA 1996, 93, 13770

[6] Sung, W.; Park, P. J. Phys. Rev. Lett. 1996, 77, 783; Muthukumar, M. J. Chem. Phys. 2003, 118, 5174; 1999, 111, 10371

[7] Marshall, B. T.; Long, M.; Piper, J. W.; Yago, T.; McEever, R. P.; Zhu, C. Nature 2003, 423, 190; Ramachandran, V.; Yago, T.; Epperson, T. K.; Kobzdej, M. M.; Nollert, M. U.; Cummings, R. D.; Zhu, C.; McEver, R. P. Proc. Natl. Acad. Sci. USA 2001, 98, 10166

[8] Leppaenen, A.; White, S. P.; Helin, J.; McEver R. P.; Cummings, R. D. J. Biol. Chem. 2000, 275, 39569; Somers, W. S.; Tang, J.; Shaw G. D.; Camphausen, R. T. Cell 2000, 103, 467

[9] de Gennes, P.-J. Scaling Concepts in Polymer Physics, 1st ed.; Cornell University Press: Ithaca, 1979; Freer, G.; Cohen-Stuart, M.; Scheutjens, J.; Cosgrove, T.; Vincent, B. Polymers at Interfaces, 1st ed.; Chapman and Hall: London, 1993

[10] Muthukumar, M. J. Chem. Phys. 1987, 86, 7230; 2004, 120, 9343; Wiegel, F. W. J. Phys. A. Math. Gen. 1977, 10, 299

[11] Ellis, M.; Kong C. Y.; Muthukumar, M. J. Chem. Phys. 2000, 112, 8723; McNamara, J.; Kong C. Y.; Muthukumar, M. ibid 2002, 117, 5354

[12] Semenov A. N.; Joanny, J. F. Europhys. Lett. 1995, 29, 279; Semenov, A. N.; Bonet-Avalos, J.; Johner, A.; Joanny, J. F. Macromolecules 1996, 29, 2179

[13] Weisel, J. W.; Shuman, H.; Litvinov, R. I. Curr. Opin. Struct. Biol. 2003, 13, 227; Liphardt, J.; Dumont, S.; Smith, S. B.; Tinoco, I.; Bustamante, C. Science 2002, 296, 1832

[14] Chang, K. C.; Tees D. F.; Hammer, D. A. Proc. Natl. Acad. Sci. USA 2000, 97, 11262; Bustanji, Y.; Arciola, R. C.; Conti, M.; Mandello, E.; Montanaro, L.; Samori, B. ibid 2003, 100, 13292

[15] Rief, M.; Clausen-Shaunman, H.; Gaub, H. E. Nat. Struct. Biol. 1999, 6, 346; Rief, M.; Gautel, M.; Schemmel, A.; Gaub, H. E. Biophys. J. 1998, 75, 3008;

[16] Ha, T.; Zhuang, X.; Kim, H. D.; Orr, J. W.; Williamson J. R.; Chu, S. Proc. Natl. Acad. Sci. USA 1999, 96, 9077; Zhuang, X.; Bartley, L. E.; Babcock, H. P.; Russell, R.; Ha, T.; Herschlag,

D.; Chu, S. Science 2000, 288, 2048

[17] Hyeon, C.; Thirumalai, D. Proc. Natl. Acad. Sci. USA 2003, 100, 10249

[18] Barsegov, V.; Thirumalai, D. Proc. Natl. Acad. Sci. USA 2005, 102, 1835; Barsegov, V.; Thirumalai, D. Phys. Rev. Lett. (in press)

[19] Bustamante, C.; Marko, J. F.; Siggia, E. D.; Smith, S. Science 1994, 265, 1599; Smith, D. E.; Chu, S. ibid 1998, 281, 1335; Perkins, Th. T.; Smith, D. E.; Chu, S. ibid 1997, 276, 2016

[20] Schurr, F.; MacKintosh, F. C.; Williams, D. R. M. Europhys. Lett. 2000, 51, 279; Montesi, A.; Pasquali M.; MacKintosh, F. C. Phys. Rev. E 2004, 69, 021916

[21] Bouchiat, C.; Mezard, M. Phys. Rev. Lett. 1998, 80, 1556; Marko, J.; Siggia, E. D. Macromolecules 1995, 28, 8759; Wilhelm, J.; Frey, E. Phys. Rev. Lett. 1996, 77, 2581

[22] Samuel, J.; Sinha, S. Phys. Rev. E 2002, 66, 050801; Krishna, M. M. G.; Samuel, J.; Sinha, S. J. Phys. A 2000, 33, 5965

[23] Lifshitz, I. M. Zh. Eksp. Teor. Fiz. 1968, 55, 2408; Grosberg, A. Yu. Biofizika 1979, 24, 32 (Biophysics 1979, 24, 30)

[24] Kierfeld, J; Lipowsky, R. J. Phys. A: Math. Gen. 2005, 38, L155

[25] Post, C. B.; Zimm, B. H. Biopolymers 1979, 18, 1487; Bloomfield, V. A. ibid 1997, 44, 269

[26] Noguchi, H; Yoshikawa, K. J. Chem. Phys. 2000, 113, 854; Sakaue, T.; Yoshikawa, K. ibid 2002, 117, 6323

[27] Kuznetsov, D. B.; Sung, W. J. Chem. Phys. 1997, 107, 4729; Macromolecules 1998, 31, 2679

[28] Semenov, A. N. Eur. Phys. J. E 2002, 9, 353

[29] Abramowitz, M.; Stegun, I. Handbook of Mathematical Functions, 9th ed.; Dover: New York, 1972.

[30] Caliskan, G. submitted to Phys. Rev. Lett.

[31] Schuler, B.; Lipman, E. A.; Steinbach, P. J.; Kumke, M.; Eaton, W. A. Proc. Natl. Acad. Sci. USA 2005, 102, 2754

[32] Murayama, Y.; Sakamaki, Y.; Sano, M. Phys. Rev. Lett. 2003, 90, 018102

[33] Lee, N.; Thirumalai, D. Eur. Phys. J. B 1999, 12, 599

FIGURE CAPTIONS

Figure 1: Schematic of a semiflexible chain (blue) adsorbed on the surface (yellow). The free end $(\mathbf{r}, \mathbf{n})$ makes an angle θ=arccos $[\mathbf{n} \cdot \mathbf{n}_x/|\mathbf{n}| \cdot |\mathbf{n}_x|]$ with the direction $\mathbf{n}_x$ of the pulling force $\mathbf{f}=f\mathbf{n}_x$. For clarity the chain is shown as extended which is realized only when the SC-surface interaction is strong. The interaction between the monomers of the chain and the surface is attractive in the range $0 \leq x \leq b$ where x is the distance perpendicular to the surface. The strength of the interaction is Δ. In the Langevin simulations we replace the square well potential by the Lennard-Jones potential (Eq. (17)).

Figure 2: Top view of the typical structures (blue) adsorbed on the surface (yellow) for S=120B, Δ=1.5B and k_BT=1.0. Extended, one-racquet, two-racquet, three-racquet and toroidal structures are obtained in a single trajectory that is terminated at t=4$\times 10^{-5}\tau$. The equilibrium structure under these conditions is the toroid.

Figure 3: Dependence of radius of gyration R_g/a (top left), intramolecular attractive interaction U_{LJ} (Eq. (16)), surface potential U_{ads} (Eq. (17)), and the internal energy U ($=U_{bend}+U_{bond}+U_{LJ}$) displayed as functions of time, measured in units of τ. The five curves in each panel correspond to extended (black), one-racquet (red), two-racquet (green), three-racquet (blue) and toroidal (magenta) structures of Fig. 2.

Figure 4: The average monomer density profiles $n(x)$ as a function of x/b for Δ=1.5B and k_BT=1.0 for extended, two-racquet, three-racquet and toroidal states. The left panel is for S=70B and the results for S=50B are shown on the right. Solid lines and dotted lines represent the results obtained using perturbative and exact theory, respectively.

Figure 5: Dynamics of extension x (in units of a) for a few trajectories at different values of f applied to the chain ends of structures shown in Fig. 2. Time t is expressed in units of τ. The colors correspond to the caption in Fig. 3. The values of f are displayed in the panels.

Figure 6: The averaged reduced extension $\langle x \rangle/L$ as a function of constant force f simulated for Δ=1.5B and k_BT=1.0 for structures in Fig. 2 (S=120B, top). The bottom panel shows force-extension profiles for four-, five-, seven-racquet and toroidal configurations obtained for S=30B (bottom panel). Data points for extended (four-racquet), one-racquet (five-racquet),

three-racquet (seven-racquet) and toroidal structures are given by red, green, blue and black circles, respectively. Theoretical curves for these structures are given respectively by solid, dotted, dashed and dot-dashed lines.

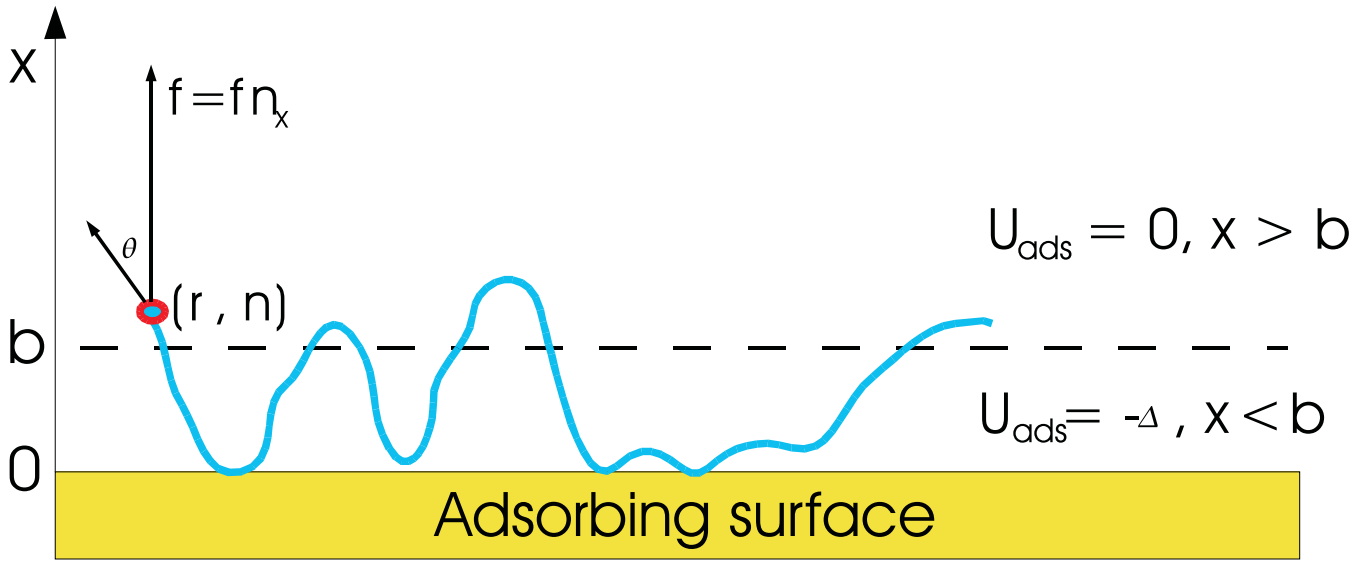

Figure 1 (V. Barsegov and D. Thirumalai)

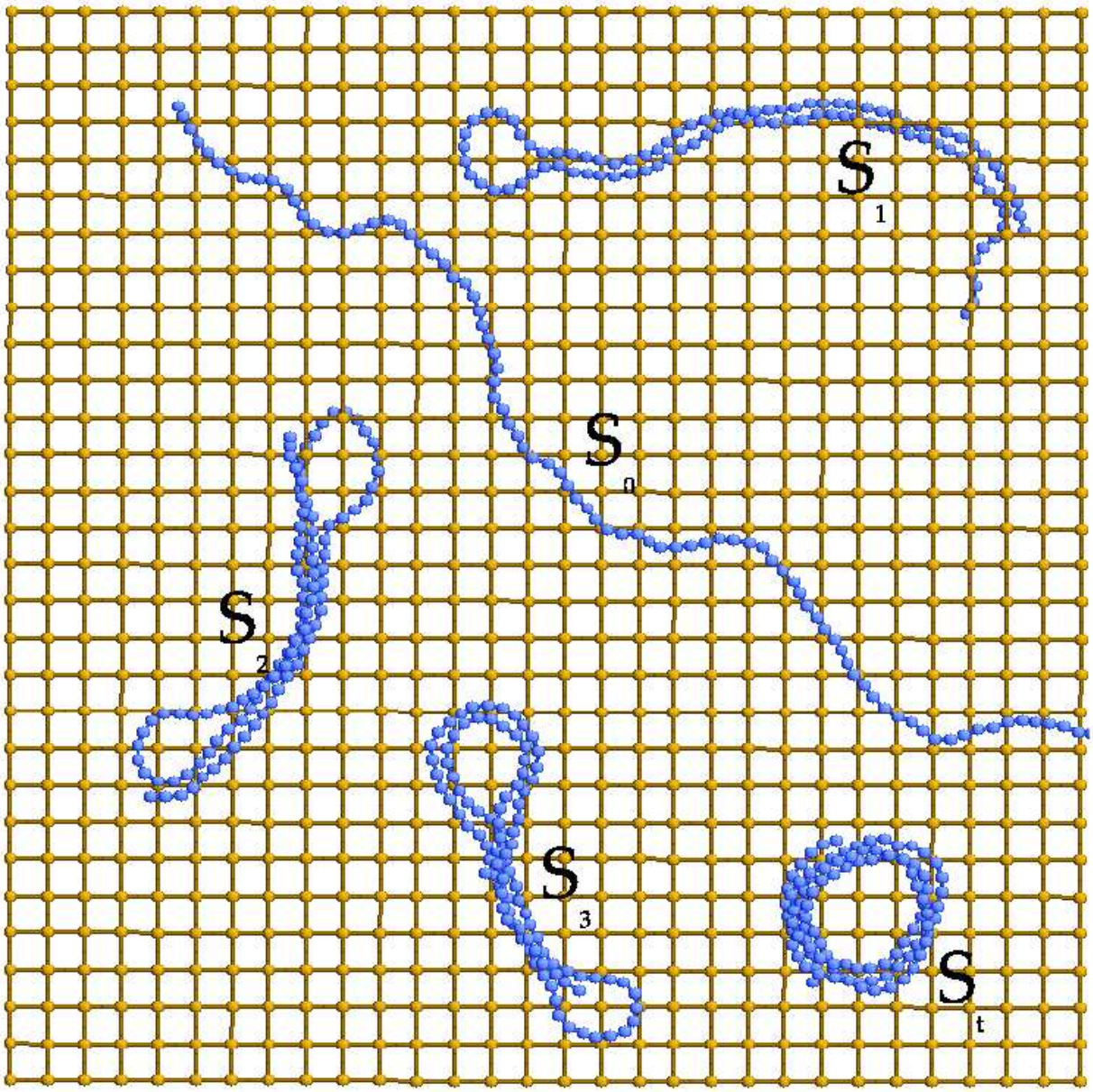

Figure 2 (V. Barsegov and D. Thirumalai)

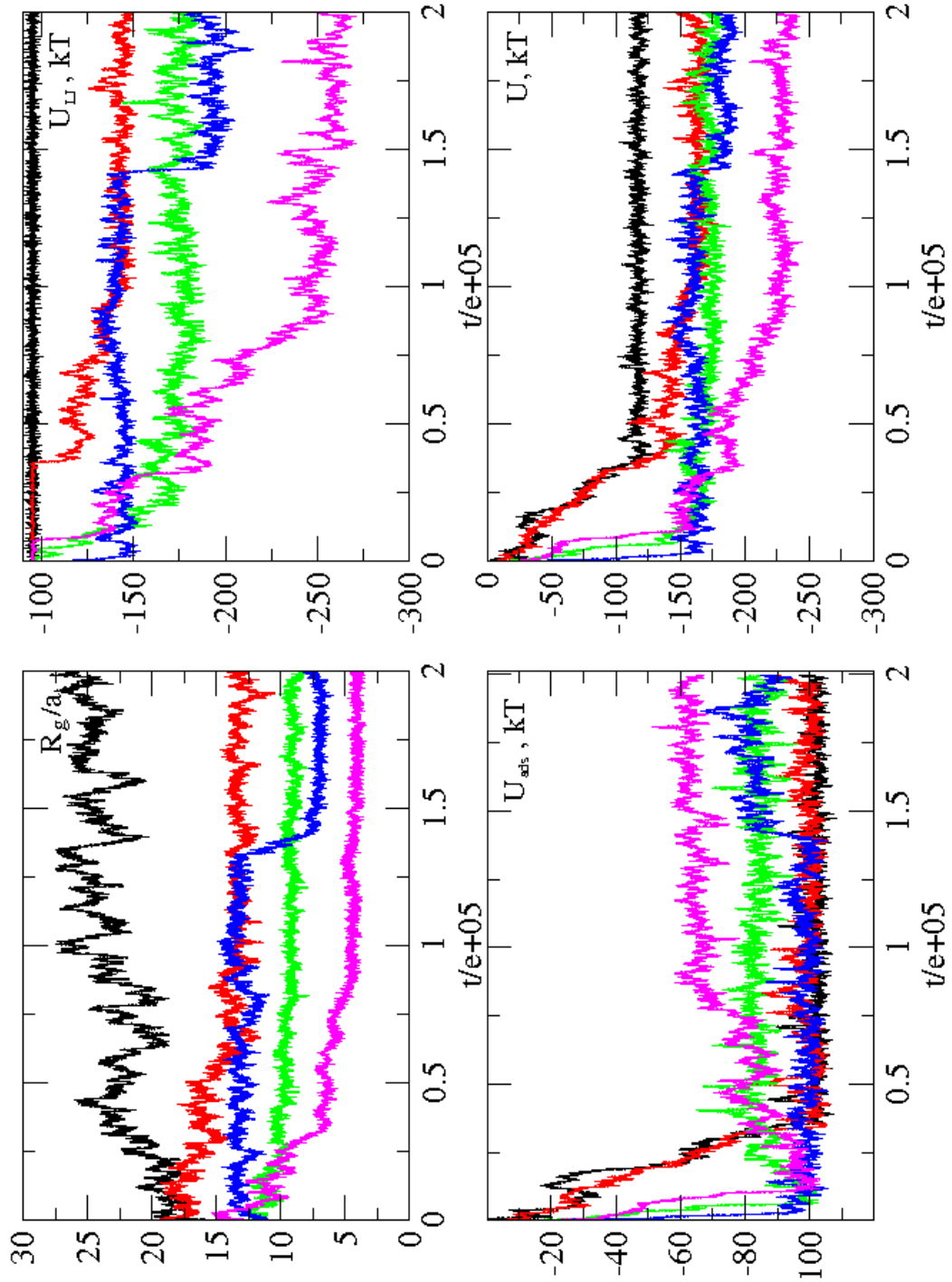

Figure 3 (V. Barsegov and D. Thirumalai)

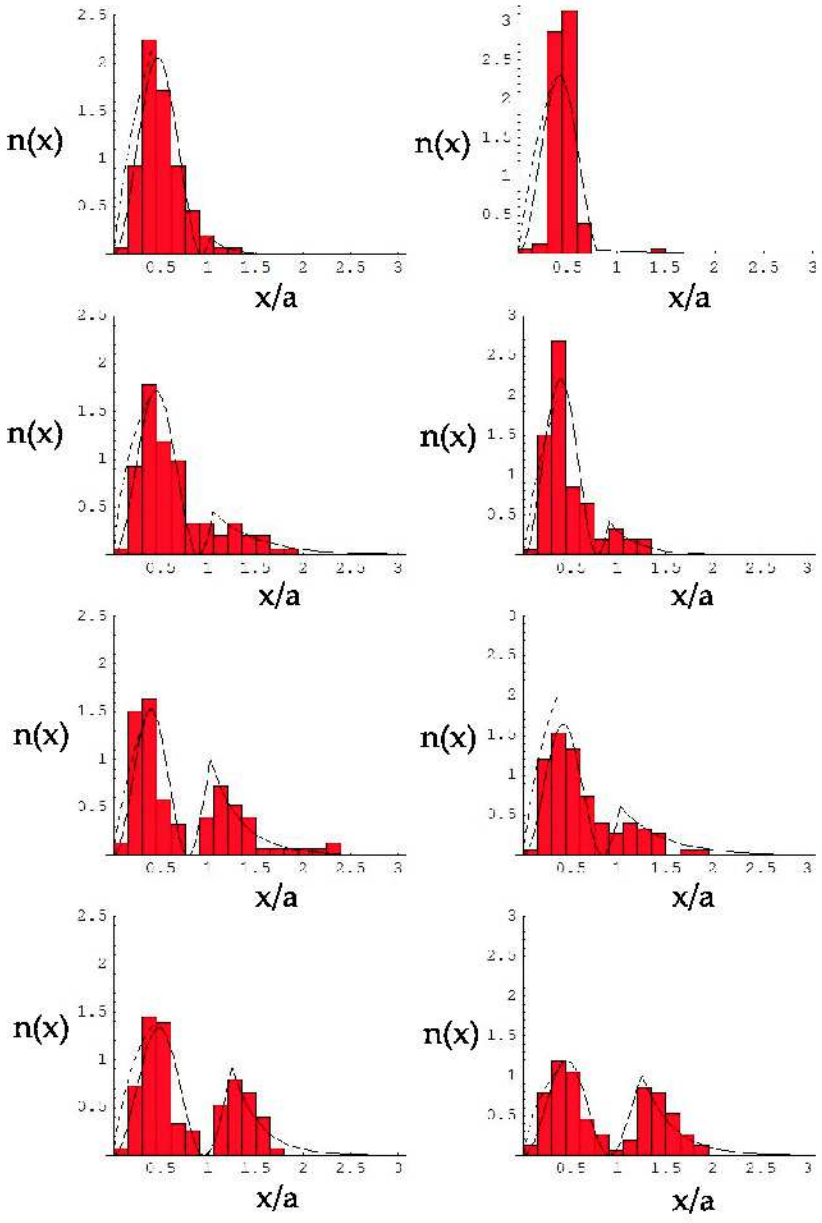

Figure 4 (V. Barsegov and D. Thirumalai)

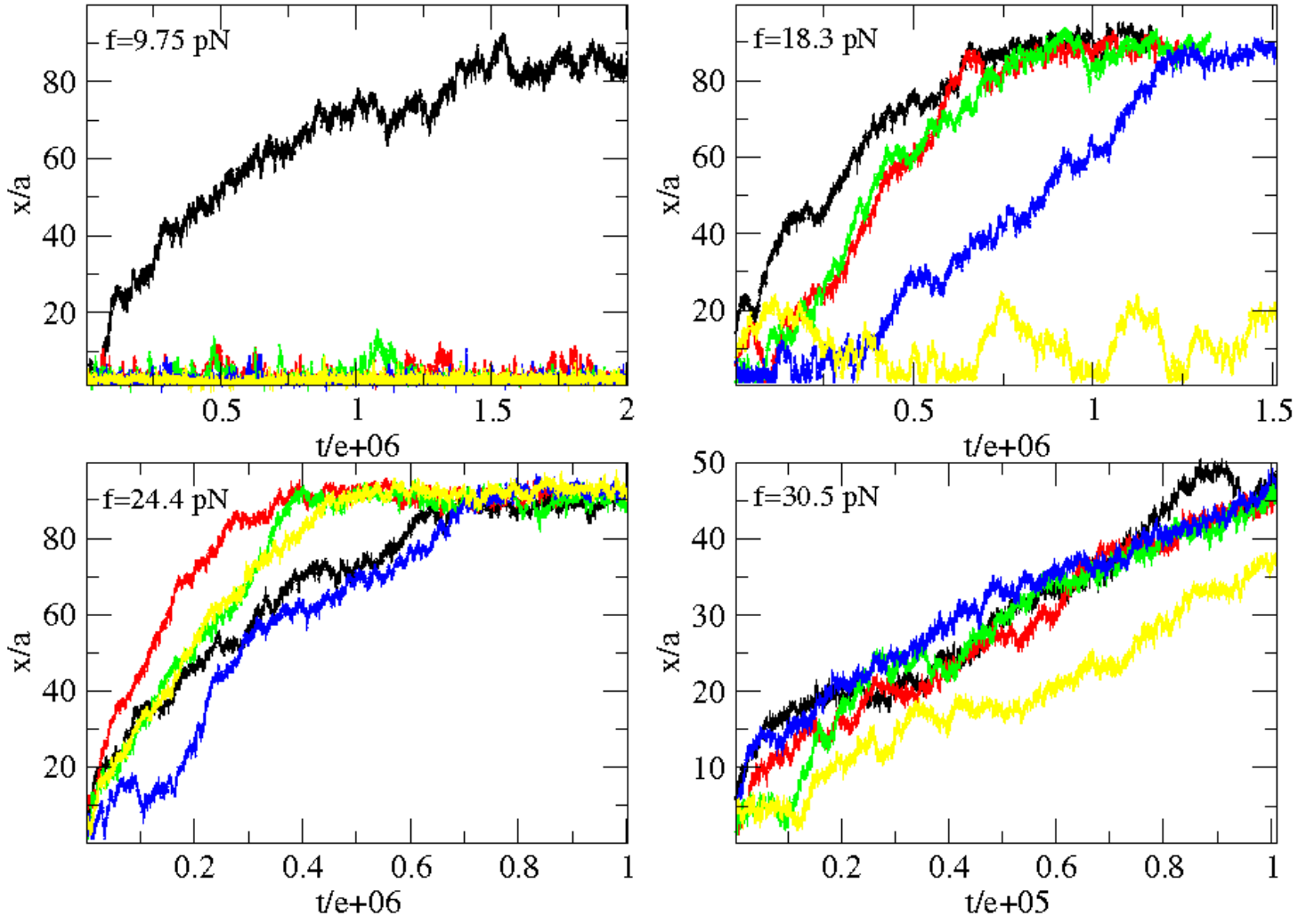

Figure 5 (V. Barsegov and D. Thirumalai)

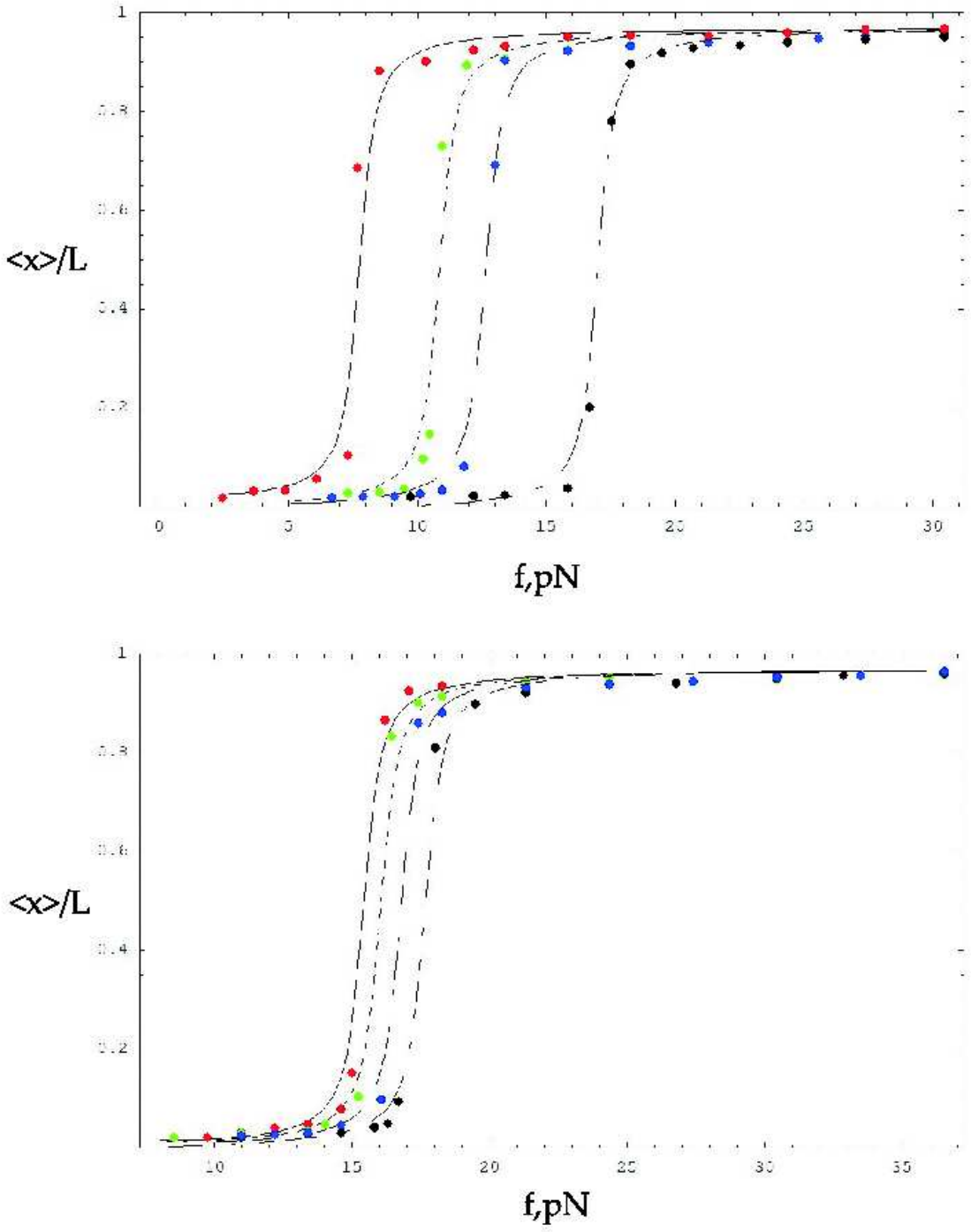

Figure 6 (V. Barsegov and D. Thirumalai)